UCSF
UC San Francisco Previously Published Works

Title

LSR/angulin-1 is a tricellular tight junction protein involved in blood–brain barrier formation

Permalink

https://escholarship.org/uc/item/7cv334jj

Journal

Journal of Cell Biology, 208(6)

ISSN

0021-9525

Authors

Sohet, Fabien
Lin, Christina
Munji, Roeben N
et al.

Publication Date

2015-03-16

DOI

10.1083/jcb.201410131

Peer reviewed

LSR/angulin-1 is a tricellular tight junction protein involved in blood–brain barrier formation

Fabien Sohet,[1,2] Christina Lin,[3] Roeben N. Munji,[1,2] Seo Yeon Lee,[3] Nadine Ruderisch,[3] Allison Soung,[1,2] Thomas D. Arnold,[4] Nikita Derugin,[5] Zinaida S. Vexler,[5] Frances T. Yen,[6] and Richard Daneman[1,2]

[1]Department of Pharmacology and [2]Department of Neuroscience, University of California, San Diego, La Jolla, CA 92093
[3]Department of Anatomy, [4]Department of Pediatrics, and [5]Department of Neurology, University of California, San Francisco, San Francisco, CA 94143
[6]Unité de Recherche Animal et Fonctionnalités des Produits Animaux (URAFPA), EA3998, Université de Lorraine, 54000 Nancy, France

THE JOURNAL OF CELL BIOLOGY

The blood–brain barrier (BBB) is a term used to describe the unique properties of central nervous system (CNS) blood vessels. One important BBB property is the formation of a paracellular barrier made by tight junctions (TJs) between CNS endothelial cells (ECs). Here, we show that Lipolysis-stimulated lipoprotein receptor (LSR), a component of paracellular junctions at points in which three cell membranes meet, is greatly enriched in CNS ECs compared with ECs in other nonneural tissues. We demonstrate that LSR is specifically expressed at tricellular junctions and that its expression correlates with the onset of BBB formation during embryogenesis. We further demonstrate that the BBB does not seal during embryogenesis in *Lsr* knockout mice with a leakage to small molecules. Finally, in mouse models in which BBB was disrupted, including an experimental autoimmune encephalomyelitis (EAE) model of multiple sclerosis and a middle cerebral artery occlusion (MCAO) model of stroke, LSR was down-regulated, linking loss of LSR and pathological BBB leakage.

Introduction

Blood vessels play a critical role in the delivery of oxygen and nutrients throughout the body. The capillary bed of each tissue is comprised of endothelial cell (ECs), which form the walls of the blood vessels, and pericytes, which sit on the abluminal surface of the endothelial tube. In the central nervous system (CNS), ECs contain a series of specialized properties, termed the blood–brain barrier (BBB), that allows them to protect neural cells from blood-borne toxic molecules, pathogens, and fluctuations of ion concentrations. CNS ECs are held together by tight junctions (TJs), which generate a tight paracellular barrier, undergo extremely low rates of transcytosis, and contain highly specific transport mechanisms. Together, these properties allow CNS ECs to tightly regulate the movement of solutes between the blood and the brain (Daneman, 2012; Siegenthaler et al., 2013; Sohet and Daneman, 2013). Loss of these barrier properties in different diseases including multiple sclerosis (MS), stroke, Alzheimer's disease, and epilepsy can lead to neuronal dysfunction and degeneration (Daneman, 2012). Thus, understanding the molecular mechanisms that regulate barrier properties might help in the discovery of new therapeutic targets that could help restore the BBB in patients with different neurological diseases.

The formation of the paracellular TJs is critical for this barrier, as it generates polarized cells with distinct luminal and abluminal composition, allowing transport properties to determine the movement of molecules across the cell barrier. TJs, first characterized by studies in epithelial cells, are formed by intercellular adhesions between the transmembrane proteins claudins, occludin, and junctional adhesion molecules (JAMs), which are linked to the cytoskeleton and adherens junctions by adaptor molecules such as zonula occludens (ZO) proteins. Claudins, a family of tetraspanin genes with >20 members in mammals (Günzel and Yu, 2013), form homotypic and heterotypic interactions that are critical for the paracellular barrier in different epithelial cells. Claudins are expressed in a tissue-specific manner, and the specific claudin family member determines the specific permeability of the TJ in each tissue. Claudin 5 is the major TJ protein expressed in ECs, and *Cldn5* knockout mice die at birth with a BBB leaky to small molecules

The Rockefeller University Press $30.00
J. Cell Biol. Vol. 208 No. 6 703–711
www.jcb.org/cgi/doi/10.1083/jcb.201410131

JCB 703

(<800 D; Nitta et al., 2003). Claudin 5 is expressed by ECs in many tissues and thus its expression alone does not confer the high resistance barrier that is specific to CNS ECs (Morita et al., 1999). Claudin 3 and claudin 12 have also been described in CNS ECs (Nitta et al., 2003; Liebner et al., 2008); however, their exact roles remain to be investigated. Occludin, also a tetraspanin, is expressed in all epithelial cells and its expression in ECs is enriched in the barrier containing ECs of the CNS (Hirase et al., 1997; Daneman et al., 2010a). Occludin-deficient mice, however, do not exhibit BBB leakage, only calcification of the brain (Saitou et al., 2000). Thus, although several components of the BBB TJs have been identified, it remains unclear why CNS ECs, but not ECs in other tissues, form these high-resistance TJs.

Ikenouchi et al. (2005) described tricellulin, a new subtype of TJ protein expressed in epithelial cells at points where three cells meet. More recently, in epithelial cells, Lipolysis-stimulated lipoprotein receptor (LSR) was described as a tricellular TJ protein required to recruit tricellulin to the epithelial tricellular TJs (Masuda et al., 2011). LSR contains an extracellular N-terminal Ig domain followed by a single transmembrane region and a cytoplasmic C-terminal tail (Stenger et al., 2012a). The original role of the protein was described in lipid metabolism studies, as LSR was first discovered to be expressed in hepatocytes, where it plays a role in the clearance of triglyceride-rich lipoproteins and low-density lipoproteins, and also acts as a apolipoprotein B/E–containing lipoprotein receptor (Stenger et al., 2012a). *Lsr* knockout mice die before embryonic day 15.5 (E15.5), but the cause of death remains unclear (Mesli et al., 2004). Two additional members of the tricellular TJ family were described in mice epithelial cells, both LSR-related proteins: immunoglobulin-like domain containing receptor ILDR1 and ILDR2 (Higashi et al., 2013). LSR, ILDR1, and ILDR2 share a complementary expression in many epithelium and all recruit tricellulin. Therefore, these three proteins have been named the angulin family, with angulin-1 (LSR), angulin-2 (ILDR1), and angulin-3 (ILDR2).

Previously, using EC purification and microarray analysis, we were able to compare the gene expression of CNS ECs with ECs from the liver and lung, identifying a dataset of BBB-enriched genes (Daneman et al., 2010a). Interestingly, tricellulin and LSR were both enriched in CNS ECs compared with peripheral ECs, which suggests that tricellular junctions may be critical for the formation of the BBB. Here, we find that LSR is expressed at the tricellular TJ in mice brain and spinal cord (SC) ECs, but not in ECs in peripheral tissues. We describe LSR expression during development and show that it follows CNS angiogenesis and correlates with BBB formation during embryogenesis. Using dye injections into developing embryos, we show that in wild-type mice the BBB seals during embryonic development at E14.5, whereas in *Lsr* knockout embryos the BBB fails to seal and is leaky to small molecule tracers. We further demonstrate that in experimental autoimmune encephalomyelitis (EAE) and middle cerebral artery occlusion (MCAO), murine models of neurological disorders in which BBB is disrupted, LSR is down-regulated in CNS ECs. Collectively, these data identify a critical role of LSR for proper BBB formation and function.

Results and discussion

LSR is expressed at tricellular TJs in CNS ECs

We first examined LSR expression in different organs by immunostaining tissue sections of brain, liver, lung, and intestine for LSR and double-labeling for ECs with an antibody directed against CD31 (Fig. 1 A). In each of these organs there is robust LSR expression. However, LSR expression only colocalizes with CD31^{+} ECs in the brain and not in the peripheral organs. In the peripheral tissues, LSR staining is restricted to epithelial cells (lung, intestine) or hepatocytes (liver). These results confirm that *Lsr* is highly enriched in brain ECs compared with liver, lung, and intestinal ECs.

To precisely define LSR sublocalization, we performed triple-labeling of mouse brain tissue sections with BSL I (to label endothelial membranes), occludin (a marker of the bicellular TJ), and LSR. High-magnification images demonstrate that occludin stains bicellular TJ, whereas LSR has a punctate expression localized to points where multiple occludin bicellular TJs meet, i.e., the tricellular junction (Fig. 1 B). Although LSR is largely enriched at the tricellular junction, lower expression levels can also be observed at the bicellular junctions. We observed the same expression pattern throughout the mouse brain and SC in all capillaries, arteries, and veins (Fig. S1 A), with the notable exceptions of the vessels in the choroid plexus and circumventricular organs. In the choroid plexus, LSR is localized at tricellular TJ of the tight epithelial cells but is absent from the leaky vessels (Fig. S1 B). LSR expression is also absent from the ECs of the circumventricular organs, which contain leaky vessels that are not part of the BBB (Fig. S1 A). Therefore, LSR protein in CNS ECs is largely expressed at the tricellular junctions of BBB-possessing vessels, which confirms a similar recent observation (Iwamoto et al., 2014).

We sought to determine the time course of LSR expression during development. Angiogenesis in the mouse CNS initiates at E9, and proceeds in a caudal-to-rostral direction. We examined LSR expression in the CNS of embryos from E10 onwards (Fig. 2). At E11.5, LSR is expressed throughout the cellular membrane of CNS ECs only at the caudal part of the SC. By E12.5, LSR expression is still diffuse throughout the EC membrane, but is expressed in vessels throughout the caudal–rostral axis of the SC and is absent from forebrain ECs. At E13.5, LSR is expressed in all blood vessels throughout the CNS including the brain, but this expression still appears to be diffuse throughout the EC membrane. Thus, LSR expression follows angiogenesis in a caudal-to-rostral direction from E11.5 to E13.5. At postnatal day 3 (P3), LSR is localized mainly at the bicellular/tricellular TJs, whereas at P12 the protein is further accumulated at the tricellular TJ and by P21 the protein is largely enriched at the tricellular junction as it is in the adult (Fig. S1 C and Fig. 1 B). Our results indicate that CNS EC expression of LSR follows slightly behind CNS angiogenesis, and as development proceeds more LSR is concentrated at the tricellular TJ of CNS blood vessels.

Lsr is made of 10 exons with three different splice variants: α, α′, and β (Yen et al., 2008; Stenger et al., 2012a). The
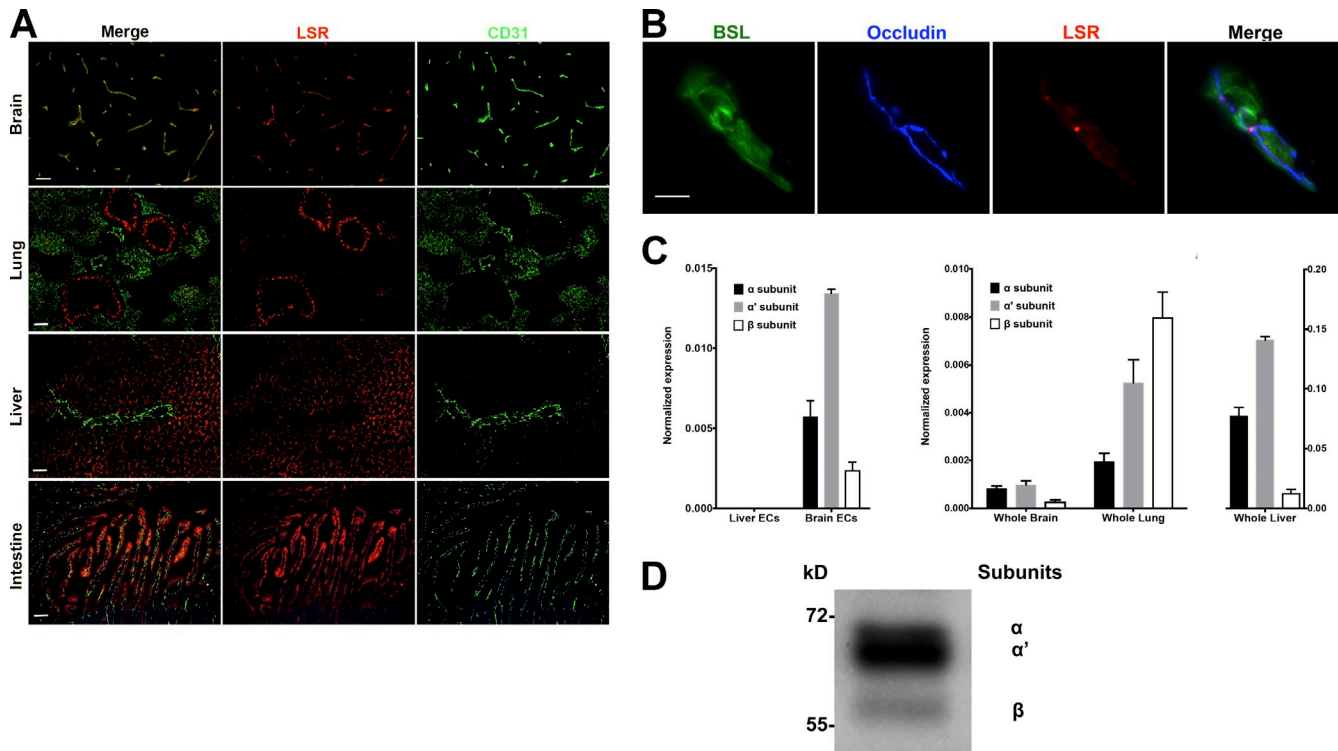
Figure 1. **LSR expression in adult mice.** (A) Tissue sections of brain, lung, liver, and intestine were colabeled with antibodies directed against LSR (red) and CD31 (green, to label blood vessels). Expression of LSR in CD31+ ECs is only observed in the brain. Bar, 100 μm. (B) Tissue sections from adult mice were labeled with the blood vessel marker BSL I (green), and antibodies against occludin (blue, bicellular TJ) and LSR (red). The merged image indicates that in CNS blood vessels LSR is localized at the tricellular TJ where two bicellular TJ meet. Bar, 5 μm. (C, left) Quantitative real-time PCR analysis of LSR isoforms from purified brain ECs and liver ECs. Analysis indicates no detectable LSR expression in liver ECs but high expression of the α′ variant followed by α and β variants in brain ECs. (C, middle and right) Quantitative real-time PCR analysis of LSR variants from whole brain, lung, and liver. The expression in liver is much higher than brain or lung, and thus was given its own y axis (right). Splice variant composition is similar between brain and liver (α′ variant followed by α and β variants) but different in the lung (β variant followed by α′ and α variants). Data represent means ± SD (error bars) from three indipendent experiments. (D) Western blot profile of LSR from purified brain capillaries shows a stronger band for the α′ splice variant followed by α and β.

α splice variant translates a full-length protein that has an external C terminus, a transmembrane domain, and a cytoplasmic N-terminal tail. The α′ and β splice variants lack a putative dileucine signal, and the β lacks almost the entirety of the transmembrane domain. The association of α/α′/β is important in the binding of lipoproteins in the liver (Yen et al., 1999, 2008). We assessed LSR splice variant composition in purified CNS ECs by qRT-PCR and identified that the main LSR splice variant is α′ followed by α and lastly β (Fig. 1 C). No LSR mRNA was detectable in purified liver ECs, which is consistent with the immunohistochemistry results (Fig. 1 A). We confirmed this data by Western blot analysis on purified mouse brain capillaries (Fig. 1 D) where the main band corresponds to α′ (64 kD), the α band has a lower density (66 kD), and the β has the weakest signal (58 kD). To compare LSR splice variant expression between different organs, we performed qRT-PCR from whole brain, lung, and liver (Fig. 1 C). In the liver, LSR is expressed primarily in hepatocytes, with α′ being the main LSR variant, followed by α and β, similar to the brain but with much higher expression levels. In the lung, LSR is expressed in epithelial cells, with β being the main LSR splice variant followed by α′ and then α. This structural difference might define a distinct function of LSR in different cell types.

## The importance of *Lsr* gene inactivation for BBB formation

To understand the physiological role of LSR at the BBB, we compared the structure and function of CNS ECs in Lsr$^{-/-}$, Lsr$^{+/-}$, and Lsr$^{+/+}$ mice. Lsr$^{-/-}$ mice have been previously generated and display embryonic lethality before E15.5 (Mesli et al., 2004). Lsr$^{-/-}$ embryos have a smaller liver and present dorsal skin detachment, but the exact cause of death remains unclear. Lsr$^{+/-}$ mice are born in a Mendelian ratio but have high plasma triglyceride and cholesterol levels during the postprandial phase (Yen et al., 2008).

The key question is to determine whether the barrier function of the CNS blood vessels is compromised in the Lsr$^{-/-}$ or Lsr$^{+/-}$ embryos. To determine if small molecules can cross the BBB in Lsr$^{-/-}$ or Lsr$^{+/-}$ embryos, we developed a method to assess BBB permeability to dyes in dissected embryos. It has been demonstrated that the BBB is functional during embryogenesis (Daneman et al., 2010b; Ben-Zvi et al., 2014); here we performed a time course examining precisely at which time point the BBB seals during embryonic development. To achieve this, we performed tracer injections on dissected embryos to determine the time course of BBB leakage during early embryogenesis. We performed Caesarean sections of pregnant females, extracted

Figure 2. LSR expression during embryogenesis. Tissue sections of E11.5 (top), E12.5 (middle), and E13.5 (bottom) mouse embryos were stained with antibodies directed against LSR (red) and CD31 (green). Whole embryos, as well as high-power images of three CNS regions (caudal SC, rostral SC, and forebrain), are shown as well as single-channel images for LSR staining. At E11.5, LSR staining is visualized in CNS blood vessels at the caudal part of the SC only. By E12.5, LSR is expressed throughout the caudal-to-rostral axis of the SC, but not in the forebrain. At E13.5, LSR is expressed in all blood vessels throughout the CNS. Bars: (left) 1.25 mm; (right) 20 µm.
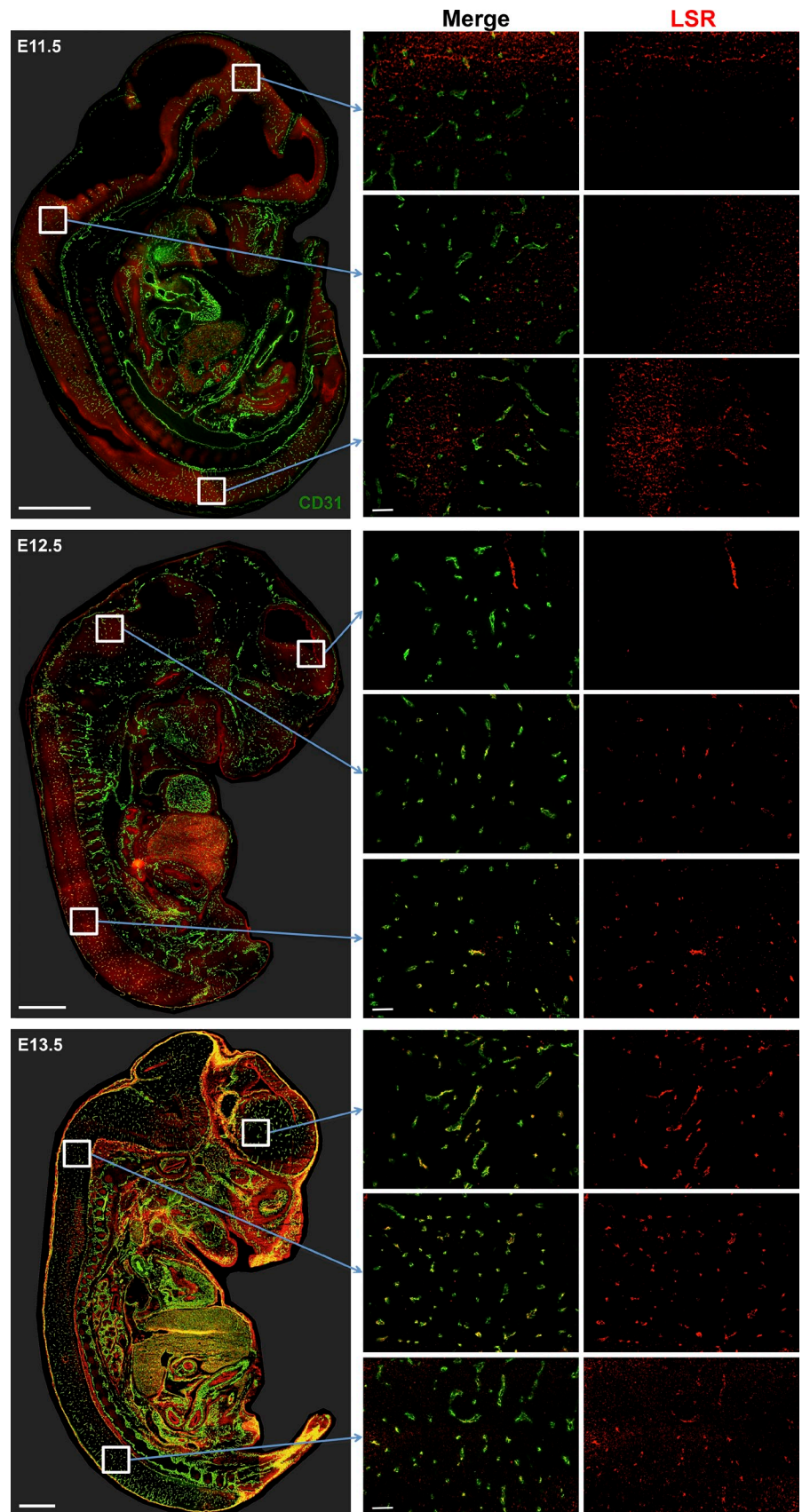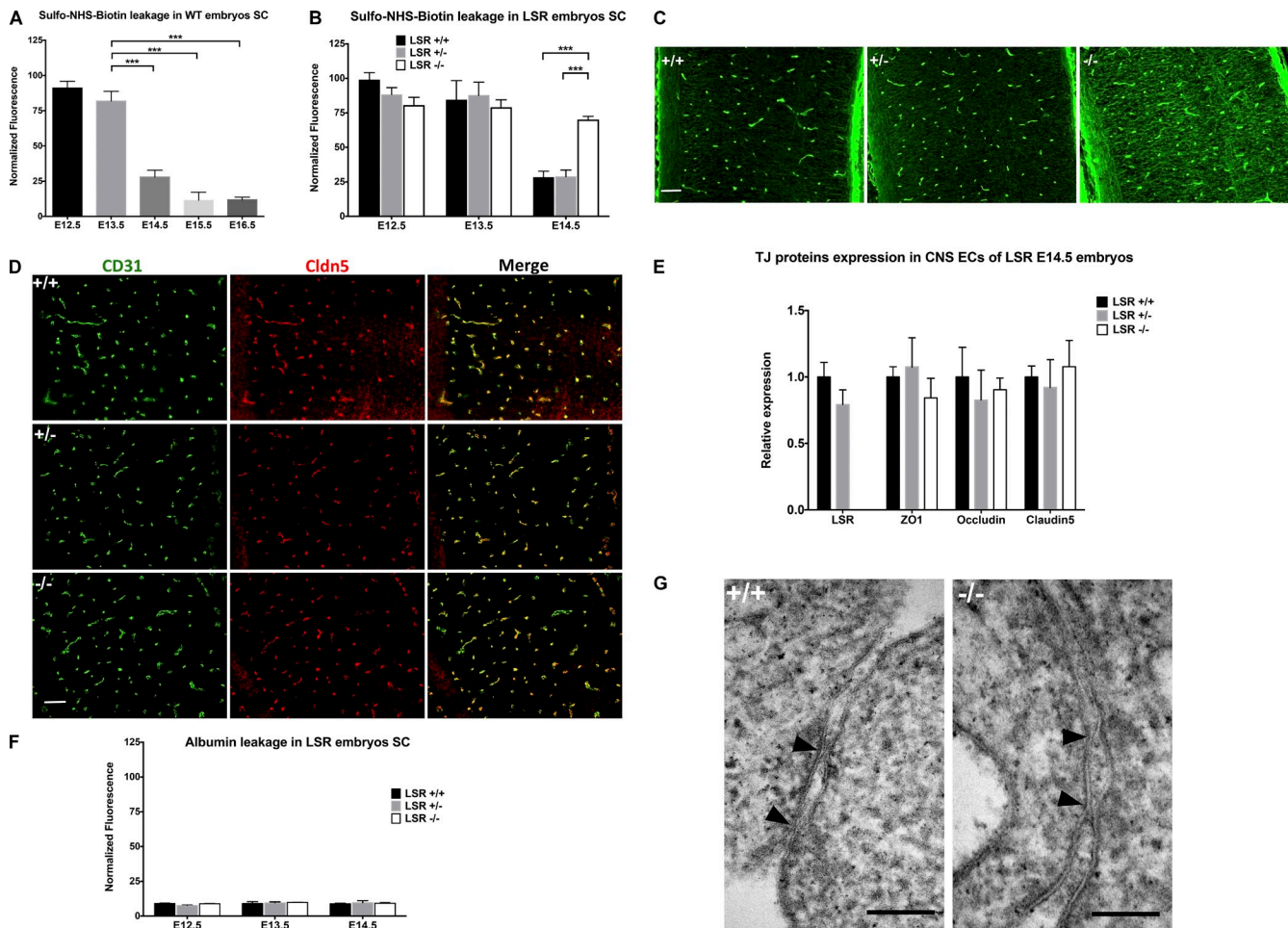
Figure 3. **BBB phenotype of LSR embryos.** (A) Quantification of Sulfo-NHS biotin leakage through the BBB of wild-type embryos at different ages. At E12.5 and E13.5, biotin leaks through the BBB. From E14.5 and onwards, leakage of Sulfo-NHS biotin is greatly restricted. (B) Quantification of BBB leakage of Sulfo-NHS biotin in Lsr$^{+/+}$, Lsr$^{+/-}$, and Lsr$^{-/-}$ embryos at E12.5, E13.5, and E14.5. At E12.5 and E13.5, Sulfo-NHS biotin leakage is comparable between the genotypes. However, at E14.5 Sulfo-NHS biotin leakage is greatly diminished in Lsr$^{+/+}$ and Lsr$^{+/-}$, but not Lsr$^{-/-}$, mice. Data represent mean ± SEM (error bars). ***, P < 0.0001. (C) Visualization of BBB leakage of Sulfo-NHS biotin in Lsr$^{+/+}$, Lsr$^{+/-}$, and Lsr$^{-/-}$ E14.5 embryos. PFA fixed tissue sections of E14.5 Sulfo-NHS biotin-injected embryos were stained with fluorophore (Alexa Fluor 488)-conjugated streptavidin. Lsr$^{+/+}$ (left) and Lsr$^{+/-}$ (middle) embryos present minimal leakage of Sulfo-NHS biotin from the blood vessels into the SC, whereas the dye is observed throughout the neural tissue of Lsr$^{-/-}$ (right) embryos. Bar, 20 µm. (D) Fresh-frozen tissue sections of E13.5 mouse SC from Lsr$^{+/+}$ (top), Lsr$^{+/-}$ (middle), and Lsr$^{-/-}$ (bottom) embryos were labeled with an anti–claudin 5 antibody (red) and CD31 to stain blood vessels (green). There was no discernable difference in the claudin 5 expression level or localization between genotypes. Bar, 20 µm. (E) Quantification of TJ protein (LSR, Zo1, Occludin, Cldn5) expression in E14.5 CNS Lsr$^{+/+}$, Lsr$^{+/-}$, and Lsr$^{-/-}$ embryos. This graph shows no significant differences for levels of Zo1, occludin, and claudin 5 between genotypes. Data represent mean ± SD (error bars). *n* is between 3 and 6. (F) Quantification of albumin leakage through the BBB of Lsr$^{+/+}$, Lsr$^{+/-}$, and Lsr$^{-/-}$ embryos from E12.5 to E14.5. There was no significant difference in leakage of albumin into the brain between genotypes at any age. Data represent mean ± SD (error bars). *n* is between 3 and 8. (G) Electron micrograph of SC blood vessels from E14.5 Lsr$^{+/+}$ and Lsr$^{-/-}$ embryos. Arrowheads indicate kissing points of TJs. There were no discernable differences in the ultrastructure of TJs between genotypes. Bar, 50 nm.

single embryos that remained attached to the placenta, and injected dyes into their heart using a glass capillary needle connected to an automated syringe pump. We only analyzed data from living embryos by ensuring that the heartbeat was maintained throughout the experiment. Any embryo whose heart stopped beating during the experiment was not analyzed. We used Sulfo-NHS-biotin (446 D) as a molecular tracer and analyzed leakage by staining tissue sections with a fluorophore-conjugated streptavidin.

We first performed a time course of biotin leakage in wild-type embryos to examine BBB permeability of embryos from E12.5 to E16.5 (Fig. 3 A). This analysis reveals that the dye leaks through the BBB until E13.5 but is greatly restricted

from E14.5 to E16.5. Thus, the BBB is permeable for the first few days after the initiation of CNS angiogenesis, then it seals to this small molecule starting at E14.5. Interestingly, this is similar to the time course of LSR expression in the vessels. To confirm that our method doesn't disrupt the vasculature, we injected 10 kD rhodamine-dextran in E12.5 LSR embryos. Fig. S2 reveals minimal leakage in any of the genotypes. Thus, at E12.5, CNS ECs are permeable to small molecules but have low permeability to large molecules. These results confirm that our method can be used to assess BBB permeability in embryos without disruption of vascular integrity.

Next, we examined whether LSR expression is necessary for BBB sealing during embryogenesis. We examined the

morphology of CNS blood vessels at a time point where LSR is expressed throughout the embryo, E13.5. CD31 staining of whole mount embryos didn't reveal any major differences in the length, branching, or overall structure of CNS blood vessels or hemorrhage (unpublished data). We then examined the time course of BBB permeability in Lsr$^{+/+}$, Lsr$^{+/-}$, and Lsr$^{-/-}$ mice (Fig. 3 B). In Lsr$^{+/+}$ and Lsr$^{+/-}$ mice, the BBB is highly permeable to Sulfo-NHS-biotin at E12.5 and E13.5, but forms a much more restrictive barrier by E14.5. In contrast, in Lsr$^{-/-}$ mice the BBB is highly permeable to the tracer at E14.5 (Fig. 3, B and C), demonstrating that LSR is required for the sealing of the BBB. Interestingly, the BBB of Lsr$^{-/-}$ mice had minimal permeability to large endogenous proteins, including albumin (69 kD; Fig. 3 F), antibodies (160 kD), and fibrinogen (52 kD; unpublished data). Thus, there is a size-selective permeability defect of the BBB in LSR-deficient mice, similar to the one described for *Cldn5* knockout mice. This suggests a common phenotype when disrupting bicellular and tricellular TJs, where leakage of small molecules probably occurs through the paracellular barrier, and therefore it seems that leakage of larger molecules may require transcellular vesicle–mediated pathways rather than paracellular pathways. It is important to note that in this mouse model, *Lsr* is deleted throughout the organism, and thus it remains possible that the leakage of the BBB is secondary to the role of LSR in other cell types, including the liver, as liver failure has been shown to lead to BBB disruption (Thumburu et al., 2012). Electron microscopy studies will be required to determine through which part of the ECs the small molecules leak in LSR-deficient mice. We have also examined BBB permeability in Lsr$^{+/-}$ adult mice brains and did not find any leakage of a biotin tracer (unpublished data), which indicates that one copy of *Lsr* is sufficient to seal the BBB throughout life.

We then studied the effect of *Lsr* deletion on the expression of bicellular TJ proteins. At the BBB, claudin 5, occludin, and ZO1 are the main bicellular TJ proteins (Sohet and Daneman, 2013). We performed immunostaining of these TJ proteins on tissue sections of E13.5 (unpublished data) and E14.5 Lsr$^{-/-}$, Lsr$^{+/-}$, and Lsr$^{+/+}$ mouse embryos and focused our observations on the blood vessels of the SC. We observed no difference in expression or localization of claudin 5 protein between Lsr$^{-/-}$, Lsr$^{+/-}$, and Lsr$^{+/+}$ embryos at both ages (Fig. 3 D). Similarly, we found no difference in the expression or localization of occludin and ZO1 (Fig. 3 E). We have also examined each bicellular TJ protein in Lsr$^{+/-}$ and Lsr$^{+/+}$ adult mouse brain tissue sections and did not find any differences (unpublished data).

For a more precise analysis of the junctional complex architecture, we performed electron microscopy on Lsr$^{-/-}$ and Lsr$^{+/+}$ E14.5 embryos. When focusing on EC adhesions, we observed TJs with kissing points in both Lsr$^{-/-}$ and Lsr$^{+/+}$ embryos with no discernable structural difference (Fig. 3 G). Therefore, removing LSR from the junctional complex doesn't disrupt the ultrastructure of the TJs. This is similar with the electron microscopy data from the study by Nitta et al. (2003), where they described no ultrastructural differences between the CNS EC TJs in *Cldn5* knockout mice and their wild-type littermates. Thus, changes in BBB permeability can occur without changes to the ultrastructure of the junction.

TJ proteins might not only be involved in sealing an epithelium or endothelium; they might have other functions. By using different fixation methods (PFA fixed tissue), LSR expression has been visualized in specific neuronal subpopulations (Stenger et al., 2012b). By performing filipin staining, the authors demonstrated an increase in membrane-associated free cholesterol in specific brain regions of 18-mo-old Lsr$^{+/-}$ mice compared with wild-type controls. This result suggests that LSR might be important for cholesterol distribution within the brain, where it localizes in membranes of glial cells and neurons, and in myelin sheets (Dietschy and Turley, 2001). We performed a filipin stain on E14.5 LSR embryos and examined the cholesterol distribution in the CNS. The staining was homogeneous between Lsr$^{-/-}$, Lsr$^{+/-}$, and Lsr$^{+/+}$ embryos (unpublished data), and quantification showed no difference in membrane-associated free cholesterol between the groups (Fig. S3). At this age, the whole brain cholesterol concentration is very low (<2 mg/g compared with 20 mg/g in adults), which might explain why no difference was observed (Dietschy and Turley, 2004).

## LSR expression in neurological disorders

BBB disruption is a common component of many different neurological diseases including MS, stroke, trauma, and neurodegenerative disorders (Daneman, 2012). Therefore, identifying the mechanisms that lead to this disruption may lead to therapeutics that limit the progression of these diseases. Here, we examined LSR expression during EAE, a mouse model of MS, and following a transient MCAO/reperfusion (MCAO) mouse model of stroke.

4 d after the onset of symptoms of EAE, we compared inflammatory lesions to unaffected white matter in the mouse SC (Fig. 4 A). Co-labeling of immune cells (CD45) and endogenous IgG identified the locations where blood vessels had become inflamed and leaky. In these inflammatory lesions, LSR was significantly down-regulated (38 ± 3%) compared with blood vessels in unaffected regions within the same tissue section (Fig. 4 B). This suggests that BBB breakdown during EAE is associated with loss of tricellular TJ proteins.

For MCAO, mice were subjected to 2 h of occlusion of the middle cerebral artery followed by a 24-h reperfusion period. We localized the leaky blood vessels in the injured hemisphere by perfusing mice with biotin and then staining the brain sections with a fluorophore-conjugated streptavidin dye (to image the leakage; Fig. 4 C) and CD31 (to stain ECs; Fig. 4 C). After selecting areas of vascular leakage in the ipsilateral hemisphere and their nonleaky vessel counterparts in the contralateral hemisphere, we performed a stain for LSR and focused our observations in the selected area (Fig. 4 D). We observed a significant down-regulation of LSR in the ipsilateral hemisphere (Fig. 4 E). These results suggest that loss of the tricellular TJ protein LSR is associated with BBB breakdown after acute MCAO.

In conclusion, we have shown that LSR is specifically expressed at the tricellular TJs of CNS blood vessels with an expression that follows BBB maturation. As previously reported, *Lsr* knockout mice are embryonic lethal (Mesli et al., 2004), and we have identified that the CNS blood vessels of
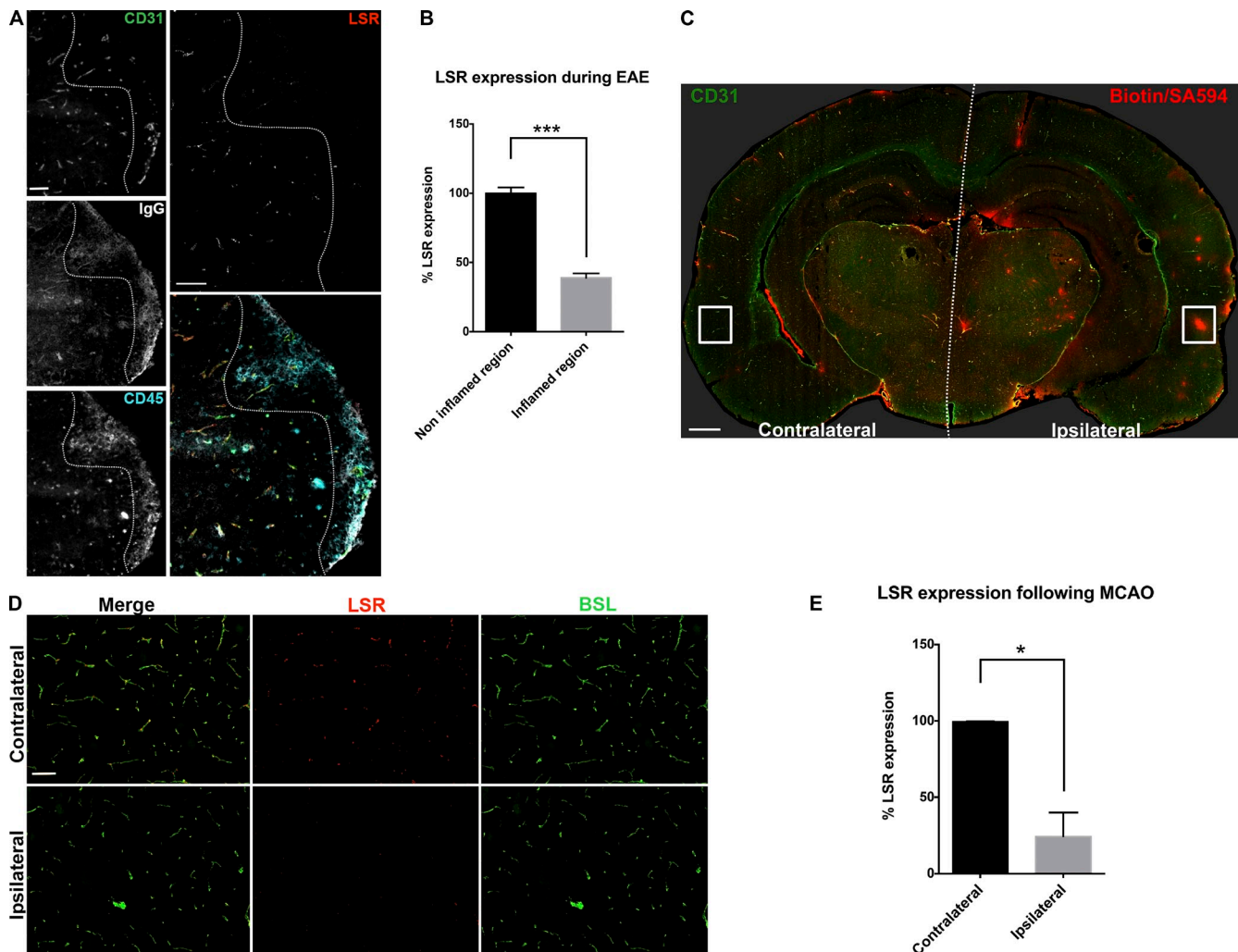
Figure 4. **LSR expression during EAE and MCAO.** (A) LSR expression in mouse SC at 4 d after onset of symptoms after induction of EAE. Tissue sections of mouse SC were labeled with antibodies against CD45 (magenta), CD31 (green), endogenous IgG (white), and LSR (red). The broken lines demarcate the inflammatory lesion on the right and the noninflamed region on the left, with larger images for LSR staining (top) and merge picture (bottom). LSR is down-regulated in inflamed blood vessels. Bars, 50 µm. (B) Quantification of LSR expression in blood vessels of inflamed and noninflamed regions after EAE induction. LSR expression is down-regulated in inflamed regions. Data represent mean ± SEM (error bars). ***, P < 0.0001. Unpaired *t* test. (C) Biotin leakage in mouse brain after MCAO. MCAO was performed on mice for 2 h, followed by 24 h of reperfusion. Mice were then anesthetized and given a transcardiac perfusion of PBS/biotin followed by PFA. Tissue sections were stained for CD31 (green) and streptavidin–Alexa Fluor 594 (to label biotin). Whole brain sections were digitally reconstructed to visualize biotin extravasation. The broken line in the center separates the contralateral hemisphere (left) from the ipsilateral side (right). Boxes indicate where pictures were taken for LSR measurement in D. Bar, 0.5 mm. (D) LSR expression in mouse brain 24 h after reperfusion after MCAO. Tissue sections of mouse brains were colabeled for LSR (red) and blood vessels (BSL, green) in the contralateral (top) and ipsilateral (bottom) hemispheres. Bar, 50 µm. (E) Quantification of LSR expression in the contralateral and ipsilateral hemispheres after MCAO. LSR expression is down-regulated in the ipsilateral hemisphere. Data represent mean ± SEM (error bars). *, P < 0.05. Unpaired *t* test.

$Lsr^{-/-}$ mice appear morphologically normal with no difference in bicellular TJ protein localization and permeability for large endogenous molecules as compared with $Lsr^{+/+}$ embryos. We have observed that wild-type embryos have leakage to small molecules for the first few days after cerebral angiogenesis, and that this barrier seals by E14.5; however, this barrier does not seal in *Lsr*-deficient embryos. This reveals an important role of LSR in proper BBB function and formation. In experimental models with a disrupted BBB, such as EAE and MCAO, LSR is down-regulated in leaky blood vessels. These results demonstrate that LSR is a BBB-enriched TJ protein that is necessary for proper BBB formation, and it is down-regulated during pathological BBB leakage associated with

neurological disorders. Collectively, these data suggest that the expression of tricellular TJ proteins by CNS ECs may be a key determinant in the formation of a high-resistance paracellular barrier.

Materials and methods

Antibodies
All antibodies are commercially available: rabbit anti-LSR (HPA007270; Sigma-Aldrich), rabbit anti–claudin 5 (34-1600; Invitrogen), rat anti-CD31 antibody (553370; BD), rabbit (40-4700; Invitrogen) and mouse (33-1500; Invitrogen) anti-occludin, mouse anti-ZO1 (33-9100; Invitrogen), rabbit anti-albumin (PA1-28339; Thermo Fisher Scientific), biotinylated rat anti-CD45 (557460; BD), and rabbit anti-fibrinogen (ab34269; Abcam).

Secondary Alexa Fluor–conjugated antibodies and fluorophore-conjugated streptavidin were all purchased from Life Technologies.

Mice
Lsr$^{+/-}$ mice were generated in the laboratory of F.T. Yen (Unité de Recherche Animal & Fonctionnalités des Produits Animaux laboratory, BFLA team, Vandoeuvre-lès-Nancy, France; Yen et al., 2008). In brief, a replacing vector that suppresses exons 2–5 of the *Lsr* gene was electroporated into 123/Ola ES cells. Targeted ES cells were injected into C57BL/6 blastocysts and implanted into C57BL/6 females. C57BL/6 mice were purchased from The Jackson Laboratory. All experimental procedures were performed according to the University of California, San Francisco, and University of California, San Diego, guidelines.

BBB permeability assays
For developmental BBB assessment, we performed a Cesarean section of pregnant females, dissected embryos from yolk sacs, and without removing the placenta placed them in room-temperature Dulbecco's PBS (DPBS). 6 µl of 1.5 mg/ml Sulfo-NHS-biotin (21217; Thermo Fisher Scientific) or 1.5 mg/ml tetramethylrhodamine-conjugated 10 kD dextran (D-1817; Life Technologies) was injected in a timespan lasting 30 s into the hearts of embryos with an automated syringe pump connected to a glass capillary needle. After a 7-min incubation time, embryos were fixed in 10% PFA for 2 h, then submerged in 30% sucrose overnight before being embedded in a 2:1 30% sucrose/OCT mixture. The heartbeat of all embryos was monitored throughout the procedure up until fixation. If the heart stopped beating before fixation, the embryos were euthanized and not used in the analysis. 10-µm sections of embryos were generated and directly imaged to visualize the injected dextran or stained with a fluorophore-conjugated streptavidin (see "Immunohistochemistry") to visualize the biotin. Images were analyzed for biotin leakage (see "Quantifications").

Immunohistochemistry
For staining of TJs proteins, embryos were frozen directly in OCT. For postnatal ages, mice were anesthetized with a ketamine (100 mg/kg) xylazine (20 mg/kg) acepromazine cocktail. They were then perfused with PBS, and their brains were dissected and frozen in OCT. 10-µm tissue sections of embryos or postnatal brains were then cut with a cryostat (Leica). Sections were fixed in 95% ice-cold ethanol for 30 min followed by incubation in acetone at room temperature for 1 min. Blocking was performed in 50% goat serum for 45 min followed by staining with primary and secondary antibodies. When indicated, fluorescein-conjugated lectin (BSL I-FL1101; Vector Laboratories) was added to the secondary antibody mixture, in which case tissue sections were postfixed for 10 min in 4% PFA after incubation with secondary antibodies.

For staining of endogenous proteins, adult mice were perfused with PBS followed by 4% PFA. Their brains were dissected, cryopreserved in 30% sucrose, and frozen in a 2:1 solution of 30% sucrose/OCT. Embryos were first injected with dyes (as described above) to study BBB permeability and then submerged into 10% PFA for 2 h, cryopreserved in 30% sucrose, and frozen in a 2:1 solution of 30% sucrose/OCT. 10-µm sections of embryos and postnatal brains were generated with a cryostat (Leica). Staining of PFA fixed tissue was performed as follows: rehydration for 5 min in PBS, blocking/permeabilization in a 50% goat serum with 0.2% of Triton-X100 for 45 min, followed by incubation with selected primary antibodies diluted in PBS containing 5% goat serum overnight at 4°C. The tissue sections were then incubated for 2 h at room temperature in specific secondary antibodies or fluorophore-conjugated streptavidin (for biotin labelling) solutions before being mounted in Vectashield with DAPI (H-1200; Vector Laboratories).

Filipin staining was performed on 4% PFA fixed embryo sections. In brief, sections were incubated in 125 µg/ml filipin diluted in 10% bovine serum albumin for 2 h at room temperature in the dark before being mounted in Vectashield without DAPI (H-1400; Vector Laboratories).

All experiments were visualized with a digital camera (Axiocam HRm; Carl Zeiss) connected to a fluorescent microscope (Axio Imager D2; Carl Zeiss). Objective lenses were: 5×, Fluor, 0.25 NA; 10×, Fluor, 0.50 NA; 20×, Plan-Apochromat, 0.8 NA; and 63×, oil, Plan-Apochromat, 1.4 NA (all from Carl Zeiss). The acquisition software used was AxioVision (Carl Zeiss), and the processing software used was Photoshop CS6 (Adobe).

Electron microscopy
For electron microscopy studies, we performed a Cesarean section of pregnant females, dissected embryos from yolk sacs, left them linked to their placenta, and placed them in room-temperature DPBS. Embryos were then perfused with a 4% formaldehyde/4% glutaraldehyde mixture. Spines were

dissected, fixed in 4% tannic acid, stained in 2% OsO4 for 1 h followed by 2% uranyl acetate for 1 h, and finally dehydrated in ethanol and embedded in epoxy resin. Ultrathin sections were cut and images were then acquired at 120 kV with a 1400 transmission electron microscope (JEOL).

EAE
C57BL/6 mice were subcutaneously injected with 200 µl of an emulsion of Complete Freund's adjuvant, MOG35-55 peptide, and inactivated mycobacterium tuberculosis (EK-2110; Hooke Laboratories). 2 h and 24 h afterwards, 200 ng of Pertussis toxin was injected i.p. (EK-2110; Hooke Laboratories). At 4 d after onset of symptoms, mice were perfused with DPBS, and their SCs were dissected and frozen in OCT. 10-µm sections were generated. Staining for LSR, CD45, CD31, and endogenous mouse IgG was performed as described in "Immunohistochemistry."

MCAO
A transient MCAO was performed in young adult C57BL/6 mice as described previously (Kokubo et al., 2002). In brief, a monofilament suture was inserted into the right external carotid artery. After 2 h of occlusion, the suture was removed. After 24 h of reperfusion, mice were perfused with DPBS followed by a solution of Sulfo-NHS-biotin (0.5 mg/ml), and their brains were dissected and bisected coronally. Half of each brain was fresh-frozen in OCT for LSR staining and the other half was postfixed for 2 h in 4% PFA for biotin labeling, cryopreserved in 30% sucrose, and frozen in a 2:1 solution of 30% sucrose/OCT. 10-µm sections were generated.

Quantifications
All quantifications were performed using Image J. To quantify leakage of endogenous molecules, the intensity of 10 different regions outside of the blood vessels was measured. The signal average was normalized to the average signal for wild-type embryos. To quantify TJ protein expression, the intensity of 10 different regions of blood vessels was measured for each TJ protein. The signal average was normalized to the average signal for wild-type embryos. To quantify leakage of biotin, the average signal intensity measured from 10 different regions outside of the blood vessels was normalized to the average signal intensity measured from 10 different regions inside the blood vessels.

Online supplemental material
Fig. S1 shows a detailed LSR expression in large vessels of the brain, at the choroid plexus, in a CVO organ, and during postnatal days. Fig. S2 shows SC tissue sections in E12.5 LSR embryos injected with a 10-kD dextran-rhodamine dye, and a graph showing leakage quantification. Fig. S3 shows a graph representing quantifications of the filipin staining in SC of E14.5 LSR embryos. Online supplemental material is available at http://www.jcb.org/cgi/content/full/jcb.201410131/DC1.

References

Ben-Zvi, A., B. Lacoste, E. Kur, B.J. Andreone, Y. Mayshar, H. Yan, and C. Gu. 2014. Mfsd2a is critical for the formation and function of the blood-brain barrier. *Nature*. 509:507–511. http://dx.doi.org/10.1038/nature13324

Daneman, R. 2012. The blood-brain barrier in health and disease. *Ann. Neurol*. 72:648–672. http://dx.doi.org/10.1002/ana.23648

Daneman, R., L. Zhou, D. Agalliu, J.D. Cahoy, A. Kaushal, and B.A. Barres. 2010a. The mouse blood-brain barrier transcriptome: a new resource for understanding the development and function of brain endothelial cells. *PLoS ONE*. 5:e13741. http://dx.doi.org/10.1371/journal.pone.0013741

Daneman, R., L. Zhou, A.A. Kebede, and B.A. Barres. 2010b. *Nature*. 468:562–566. http://dx.doi.org/10.1038/nature09513

Dietschy, J.M., and S.D. Turley. 2001. Cholesterol metabolism in the brain. *Curr. Opin. Lipidol.* 12:105–112. http://dx.doi.org/10.1097/00041433-200104000-00003

Dietschy, J.M., and S.D. Turley. 2004. Thematic review series: brain lipids. Cholesterol metabolism in the central nervous system during early development and in the mature animal. *J. Lipid Res.* 45:1375–1397. http://dx.doi.org/10.1194/jlr.R400004-JLR200

Günzel, D., and A.S. Yu. 2013. Claudins and the modulation of tight junction permeability. *Physiol. Rev.* 93:525–569. http://dx.doi.org/10.1152/physrev.00019.2012

Higashi, T., S. Tokuda, S. Kitajiri, S. Masuda, H. Nakamura, Y. Oda, and M. Furuse. 2013. Analysis of the 'angulin' proteins LSR, ILDR1 and ILDR2—tricellulin recruitment, epithelial barrier function and implication in deafness pathogenesis. *J. Cell Sci.* 126:966–977. http://dx.doi.org/10.1242/jcs.116442

Hirase, T., J.M. Staddon, M. Saitou, Y. Ando-Akatsuka, M. Itoh, M. Furuse, K. Fujimoto, S. Tsukita, and L.L. Rubin. 1997. Occludin as a possible determinant of tight junction permeability in endothelial cells. *J. Cell Sci.* 110:1603–1613.

Ikenouchi, J., M. Furuse, K. Furuse, H. Sasaki, S. Tsukita, and S. Tsukita. 2005. Tricellulin constitutes a novel barrier at tricellular contacts of epithelial cells. *J. Cell Biol.* 171:939–945. http://dx.doi.org/10.1083/jcb.200510043

Iwamoto, N., T. Higashi, and M. Furuse. 2014. Localization of angulin-1/LSR and tricellulin at tricellular contacts of brain and retinal endothelial cells in vivo. *Cell Struct. Funct.* 39:1–8. http://dx.doi.org/10.1247/csf.13015

Kokubo, Y., G.B. Matson, N. Derugin, T. Hill, A. Mancuso, P.H. Chan, and P.R. Weinstein. 2002. Transgenic mice expressing human copper-zinc superoxide dismutase exhibit attenuated apparent diffusion coefficient reduction during reperfusion following focal cerebral ischemia. *Brain Res.* 947:1–8. http://dx.doi.org/10.1016/S0006-8993(02)02899-8

Liebner, S., M. Corada, T. Bangsow, J. Babbage, A. Taddei, C.J. Czupalla, M. Reis, A. Felici, H. Wolburg, M. Fruttiger, et al. 2008. Wnt/β-catenin signaling controls development of the blood-brain barrier. *J. Cell Biol.* 183:409–417. http://dx.doi.org/10.1083/jcb.200806024

Masuda, S., Y. Oda, H. Sasaki, J. Ikenouchi, T. Higashi, M. Akashi, E. Nishi, and M. Furuse. 2011. LSR defines cell corners for tricellular tight junction formation in epithelial cells. *J. Cell Sci.* 124:548–555. http://dx.doi.org/10.1242/jcs.072058

Mesli, S., S. Javorschi, A.M. Bérard, M. Landry, H. Priddle, D. Kivlichan, A.J. Smith, F.T. Yen, B.E. Bihain, and M. Darmon. 2004. Distribution of the lipolysis stimulated receptor in adult and embryonic murine tissues and lethality of LSR-/- embryos at 12.5 to 14.5 days of gestation. *Eur. J. Biochem.* 271:3103–3114. http://dx.doi.org/10.1111/j.1432-1033.2004.04223.x

Morita, K., H. Sasaki, M. Furuse, and S. Tsukita. 1999. Endothelial claudin: claudin-5/TMVCF constitutes tight junction strands in endothelial cells. *J. Cell Biol.* 147:185–194. http://dx.doi.org/10.1083/jcb.147.1.185

Nitta, T., M. Hata, S. Gotoh, Y. Seo, H. Sasaki, N. Hashimoto, M. Furuse, and S. Tsukita. 2003. Size-selective loosening of the blood-brain barrier in claudin-5-deficient mice. *J. Cell Biol.* 161:653–660. http://dx.doi.org/10.1083/jcb.200302070

Saitou, M., M. Furuse, H. Sasaki, J.D. Schulzke, M. Fromm, H. Takano, T. Noda, and S. Tsukita. 2000. Complex phenotype of mice lacking occludin, a component of tight junction strands. *Mol. Biol. Cell.* 11:4131–4142. http://dx.doi.org/10.1091/mbc.11.12.4131

Siegenthaler, J.A., F. Sohet, and R. Daneman. 2013. 'Sealing off the CNS': cellular and molecular regulation of blood-brain barriergenesis. *Curr. Opin. Neurobiol.* 23:1057–1064. http://dx.doi.org/10.1016/j.conb.2013.06.006

Sohet, F., and R. Daneman. 2013. Genetic mouse models to study blood-brain barrier development and function. *Fluids Barriers CNS.* 10:3. http://dx.doi.org/10.1186/2045-8118-10-3

Stenger, C., C. Corbier, and F.T. Yen. 2012a. Structure and Function of the Lipolysis Stimulated Lipoprotein Receptor. *In* Chemical Biology. D. Ekinci, editor. InTech, Rijeka, Croatia. 267–292. http://dx.doi.org/10.5772/34657

Stenger, C., A. Pinçon, M. Hanse, L. Royer, A. Comte, V. Koziel, J.L. Olivier, T. Pillot, and F.T. Yen. 2012b. Brain region-specific immunolocalization of the lipolysis-stimulated lipoprotein receptor (LSR) and altered cholesterol distribution in aged LSR+/- mice. *J. Neurochem.* 123:467–476. http://dx.doi.org/10.1111/j.1471-4159.2012.07922.x

Thumburu, K.K., S. Taneja, R.K. Vasishta, and R.K. Dhiman. 2012. Neuropathology of acute liver failure. *Neurochem. Int.* 60:672–675. http://dx.doi.org/10.1016/j.neuint.2011.10.013

Yen, F.T., M. Masson, N. Clossais-Besnard, P. André, J.M. Grosset, L. Bougueleret, J.B. Dumas, O. Guerassimenko, and B.E. Bihain. 1999. Molecular cloning of a lipolysis-stimulated remnant receptor expressed in the liver. *J. Biol. Chem.* 274:13390–13398. http://dx.doi.org/10.1074/jbc.274.19.13390

Yen, F.T., O. Roitel, L. Bonnard, V. Notet, D. Pratte, C. Stenger, E. Magueur, and B.E. Bihain. 2008. Lipolysis stimulated lipoprotein receptor: a novel molecular link between hyperlipidemia, weight gain, and atherosclerosis in mice. *J. Biol. Chem.* 283:25650–25659. http://dx.doi.org/10.1074/jbc.M801027200